Emergent Materials (2024) 7:947–957
https://doi.org/10.1007/s42247-023-00619-4

ORIGINAL ARTICLE

New process for the treatment of polluted water using the coupling of nanoparticles (Fe_3O_4) and intense magnetic system

Hajer Tlili[1,2] · Anis Elaoud[2,3] · Nedra Asses[2] · Karima Horchani-Naifer[1] · Mounir Ferhi[1]

Received: 4 October 2023 / Accepted: 19 December 2023 / Published online: 29 December 2023

Abstract

This study presents an innovative approach to reducing oxidizable pollutants in contaminated water by using magnetite Fe_3O_4 nanoparticles (MNPs) in conjunction with a high-intensity magnetic field. The MNPs used as adsorbents were synthesized by co-precipitation method and analyzed by transmission electron microscopy (TEM), scanning electron microscopy (SEM), X-ray diffraction analysis (XRD), Fourier transform infrared spectroscopy (FTIR), surface area analysis (BET), and thermogravimetric analysis (TGA). The performance on the reduction efficiency of the contaminated water was investigated under different conditions: pH (4–9), adsorbent masses (0.5–1.5 g/L), contact times (15–90 min), and stirring rates (50–300 rpm). The nanoparticles produced by co-precipitation showed a smaller size than the other techniques (10 nm). The optimum results of the treatment with magnetite indicate the reduction conditions: contact time of 50 min, pH of 8, mass of magnetite of 1 g/L, and stirring speed of 200 rpm. Using the coupling of nanoparticles and an intense magnetic field (1T) generates better treatments up to 84% COD and 85% BOD_5. These results highlight the potential of this method for advanced environmental applications, offering a new way to treat polluted water.

Keywords Magnetite · Co-precipitation · Magnetic field · Water treatment · Nanoparticles

Abbreviations

BOD_5	Biological oxygen demand
COD	Chemical oxygen demand
MNPs	Magnetite nanoparticles
SEM	Scanning electron microscopy
XRD	X-ray diffraction analysis
FTIR	Fourier transform infrared
MF	Magnetic field
FWHM	Full with at half maximum
TGA	Thermogravimetric analysis
DO	Dissolved oxygen
EDX	Energy-dispersive X-ray spectroscopy

Environmental implication The environmental implication for this paper is to reduce the pollution from water, using magnetite Fe_3O_4 nanoparticles (MNPs) in combination with a high-intensity magnet. The MNPs used as adsorbents were synthesized by co-precipitation method and analyzed. Using the coupling of nanoparticles and an intense magnetic field (1T) generates a better water treatment.

✉ Mounir Ferhi
ferhi.mounir@gmail.com

1 Physical Chemistry Laboratory for Mineral Materials and Their Applications, National Center for Research in Materials Sciences CNRSM, Technopole Borj Cedria, Soliman, Tunisia

2 Laboratory of Environmental Sciences and Technologies, Higher Institute of Environmental Sciences and Technologies, Carthage University, Tunis, Tunisia

3 Laboratory of Probability and Statistics, Faculty of Sciences Sfax, University of Sfax, Sfax, Tunisia

1 Introduction

An increase in factories, industrial activity, and demographic expansion has negatively impacted the environment by producing polluted and dangerous polluted water. Contaminated water flows primarily consist of emerging contaminants, which are persistent non-biodegradable chemicals [1]. These substances linger in the environment, accumulate within food chains, and present hazards not only to human well-being but also to ecosystems and microbial populations [2–4]. The quality of water is crucial in determining its impact on human health and ecosystem equilibrium, playing a vital role in the advancement of technologies aimed at removing pollutants to support the

global water cycle. Synthetic drugs represent a significant and growing category of pollutants, with their presence in aquatic environments posing a substantial environmental risk. Their stability and resistance to biodegradation contribute to their accumulation [5].

Water polluted by toxic heavy metals is a major problem worldwide. Strict environmental regulations on heavy metal discharge and growing demand for purified water exhibiting minimal concentrations of heavy metals content have highlighted the urgent need to develop efficient heavy metal removal technologies.

Water treatment is essential to make water suitable for various uses such as domestic activities, industrial, and agricultural activities. Unfortunately, however, the polluted water treatment process itself has become an industry that pollutes the environment in various ways [6]. In the past, water treatment methods were limited, but with advances in knowledge and technology, researchers have developed environmentally friendly and effective contaminated water treatment methods [7–9].

Seham Nagib et al. propose a method for the recovery of vanadium from hydrodesulfurization waste catalysts using calix resorcinarenes, which not only offers a solution for the management of hazardous waste but also allows for the recovery of precious metals [10].

Ferrite-based systems have garnered significant attention in recent scientific and technological research, owing to their unique magnetic properties, thermal and chemical stability, and ease of synthesis. These materials have proven particularly effective in redox processes, playing an important role in various applications ranging from water treatment to environmental catalysis. Recent studies, the researchers have highlighted the efficiency of ferrites in separation and purification processes, offering innovative solutions for pollutant degradation and environmental purification. The ability of ferrites to facilitate oxidation and reduction reactions, combined with their applicability in sustainable and environmental contexts, fully justifies the choice to investigate them. This research aligns with ongoing efforts to explore the potential of ferrites in advanced scientific and technological applications, underscoring their growing importance in the development of new solutions to current environmental challenges [11–13].

The unique properties of nanosorbents offer unprecedented opportunities for the highly efficient and cost-effective metals removal. Different nanoparticles and dendrimers extensive research have been conducted to explore their potential, while magnetite nanoparticles extensive research has been conducted to investigate their potential uses in the field of biomedicine [14]. Their application in the environmental field has received limited attention in previous studies [15].

Scientific research shows that adsorption is a more efficient method used in water treatment and is increasingly used because of its affordability, convenient availability of raw materials, and decreased usage of treatment agents [16, 17]. It has the capability to eliminate not only heavy metals present in polluted water but also organic substances and various contaminants in water [18, 19]. Recent concerns focus using nanomaterials for the purpose of decreasing COD and BOD_5 levels, while taking into account ecological safety concerns [20].

Magnetite nanoparticles have gained significant popularity in contaminated water treatment, primarily due to their large specific surface area, short diffusion paths, and easily adaptable surface functional groups for targeted modifications. In addition, the use of an external magnetic field greatly enhances the separation efficiency of these nanoparticles. This not only simplifies their extraction, but also facilitates their subsequent recycling and reuse, making the process more sustainable and cost-effective [21].

Recent research has presented evidence indicating the beneficial impact of magnetic fields on wastewater treatment. Magnetic fields have also been examined in terms of their potential to safeguard human health [22].

On the other hand, numerous researchers have investigated the use of magnetic fields to treat water in various areas. For example, magnetic water treatment has been tested to see how it affects the growth of fruits and vegetables. Some studies found that using these devices led to better yields. For instance, the yield of melon crops increased by 39%, and potato yields went up by 41% (with a magnetic field strength of 0.33 T) and 52% (with a magnetic field strength of 0.29 T) compared to using untreated water [23]. Additionally, scientists have looked into how magnetic treatment affects the physical and chemical properties of water. They examined factors like pH, conductivity, surface tension, turbidity, and evaporation rate. By using magnetic devices with different strengths (0.5 and 0.29 Tesla), they found that applying a magnetic field made the water's pH decrease. This change seemed to enhance the germination rate and seed capacity before the seeds developed into seedlings [24]. Some researchers even explored the effects of magnetic treatment on melon production in areas with high soil salinity. They discovered that applying a permanent magnetic treatment lowered the water's electrical conductivity while increasing its pH. These changes led to a significant increase in melon crop yields. The researchers focused on a concept involving radical ion pairs as the entities affected by magnetic fields and the source of resulting effects. Several scientists reported that exposing irrigation water to a magnetic field prior to use improved plant productivity and altered the water and mineral metabolism of the plants [25–27]. The magnetic treatments also impacted the physical parameters

of water, such as pH and electrical conductivity. The application of a magnetic field reduced water's surface tension by up to 24% and increased the amount of water that evaporated compared to untreated water [28].

Iron oxide nanoparticles, especially magnetite (Fe3O4), are effective in water purification, as they can remove heavy metals, dyes, and organic pollutants due to their large surface area and strong adsorption capacity. They are also magnetically recoverable, making them practical for water treatment systems. The researchers indicate that adding cuprite-doped magnetite nanoparticles to epoxy coatings improves the performance of marine steel coatings, highlighting their potential application in water treatment technologies [29].

Reducing COD and BOD_5 is of utmost importance to levels that allow this sewage to be discharged into rivers. According to the ISO standard (International-Organization for the Standardization of Discharge of Sewage to the Aquatic Environment), the COD value is required to be less than $30mgO_2/L$, and the BOD_5 value is less than $250mgO_2/L$.

Today, many researchers focus on COD and BOD_5 removal using magnetite nanoparticles, for example: [30] studied COD reduction in oilfield water and regeneration using modified Fe_3O_4 nanoparticles, and furthermore used Fe_3O_4-modified composites for addressing COD in industrial polluted water. Fe_3O_4/mordenite for COD reduction in oily refinery polluted water [31]. The utilization of magnetic nanoparticle–based magnetic separation technology has been explored for the purpose of removing COD from pre-treated palm oil polluted water [32].

This study is the first focusing on diminishing BOD_5 and COD levels in water by adsorption on magnetite nanoparticles under a high magnetic intensity. Adsorption on magnetic nanoparticles is enhanced by utilization of a magnetic field through physical excitation of ions as well as molecules of nanoparticles and organic pollutants. Furthermore, the implementation of a magnetic field simplifies the separation of magnetite nanoparticles.

2 Materials and methods

2.1 Description of the samples and magnetic process

The water samples were collected from the Wadi El Bey river Tunisia situated in northeastern Tunisia, spans between latitudes 36° 35′ 00″ and 36° 42′ 00″ N, and longitudes 10° 28′ 00″ and 10° 33′ 00″ E. It encompasses an area of 475 km^2, draining into the Grombalia plain. The area experiences an average potential evapotranspiration of approximately 1300 mm per year, with higher rates in the summer due to elevated temperatures and lower MNP are employed for the treatment of polluted water in an innovative process. These particles are introduced into the water, where they act as purification agents by attaching to contaminants. A magnetic field with an intensity of 1 Tesla, generated by a device from Delta Water, is then applied. This magnetic field intensifies the effectiveness of the MNPS by enhancing their interaction with the pollutants over a period of 50 min.

2.2 Synthesis of MNPs

MNPs were prepared by the co-precipitation protocol presented in Fig. 1, following the Massart method with some modifications [33] as described below. Deionized water (20 mL) was combined with 3.5 g of iron (II) chloride to prepare the Fe^{2+} precursor solution (S1), while for a Fe^{+3} precursor solution (S2), by dissolving 8.64 g of iron (III) chloride in 20 mL of deionized water. For the third solution (S3), dissolve 7.2 g of sodium hydroxide in 100 mL of deionized water. For

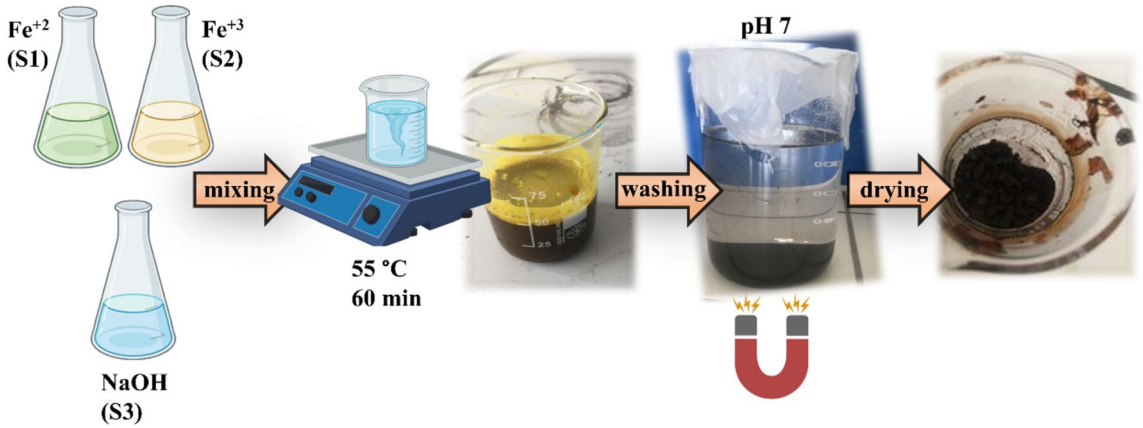

Fig. 1 Schematic representation of the followed simple synthesis route mixing Fe^{2+} (S1) and Fe^{3+} (S3) with NaOH aqueous solutions (S3) to produce magnetite nanoparticles (MNPs)

each experiment, the combined volume of the three solutions was 140 mL, and the reaction took place at 55 °C for a duration of 60 min, maintaining chemical reaction volume by adding deionized water. The obtained MNPs were magnetically decanted and washed with deionized water until they attained a neutral pH (7–8). Well-dried magnetite nanoparticles were stored for characterization as follows.

2.3 Characterization

The morphological aspect of MNPs was characterized using a FEG TECNAI T20 transmission electron microscope (TEM) at an acceleration voltage of 200 kV and Quanta FEG 650 model scanning electron microscope (SEM) at 10 kV, 120,000 of magnification, and 12.1 mm of working distance. For TEM analysis, samples were conditioned from a dilute solution containing the MNPs by dropping the colloid onto a holey carbon cupper grid to determine the morphology and particle size distribution. Statically analysis (n = 200) was performed on TEM images using ImageJ analysis software. The chemical composition of the samples was analyzed using a Perkin Elmer FTIR frontier Fourier transform infrared spectrometer. Additionally, chemical analysis was performed using an energy-dispersive X-ray (EDX) detector on a Quanta FEG 650 model scanning electron microscope (SEM) operating at 10 kV. The crystal structure of the resulting product was investigated using a Bruker D8 Advance high-resolution X-ray powder diffractometer (XRD) with Cu-K radiation. (1.5418 Å).

3 Results and discussion

3.1 MNP characterization

3.1.1 Electron microscopy analysis

TEM analysis revealed partially agglomerated particles with an average particle size = 10 ± 2 nm (Fig. 2a). The histogram of the static sample analysis (n = 200) is shown in Fig. 2b. It was previously reported that nanoparticle agglomeration was induced by van der Waals forces arise due to operating conditions and the drying process. The existence of remaining water and NaOH facilitated the clustering of nanoparticles due to a nanometer size in the tens of nanometers.

The SEM image (Fig. 2c) confirmed the agglomeration in cumulus over 500 nm and EDS spectrum (Fig. 2d) shown clearly the elemental contributions from Fe_L (0.705 eV), O_K (0.523 eV), and C_K (0.523 eV) present in the sample. According to the table of elemental analysis result, the sample contains 72.94% Fe and 24.68% O in mass. The presence of 2.38% of carbon can be attributed to the utilization of carbon tape for securing the sample to the holder.

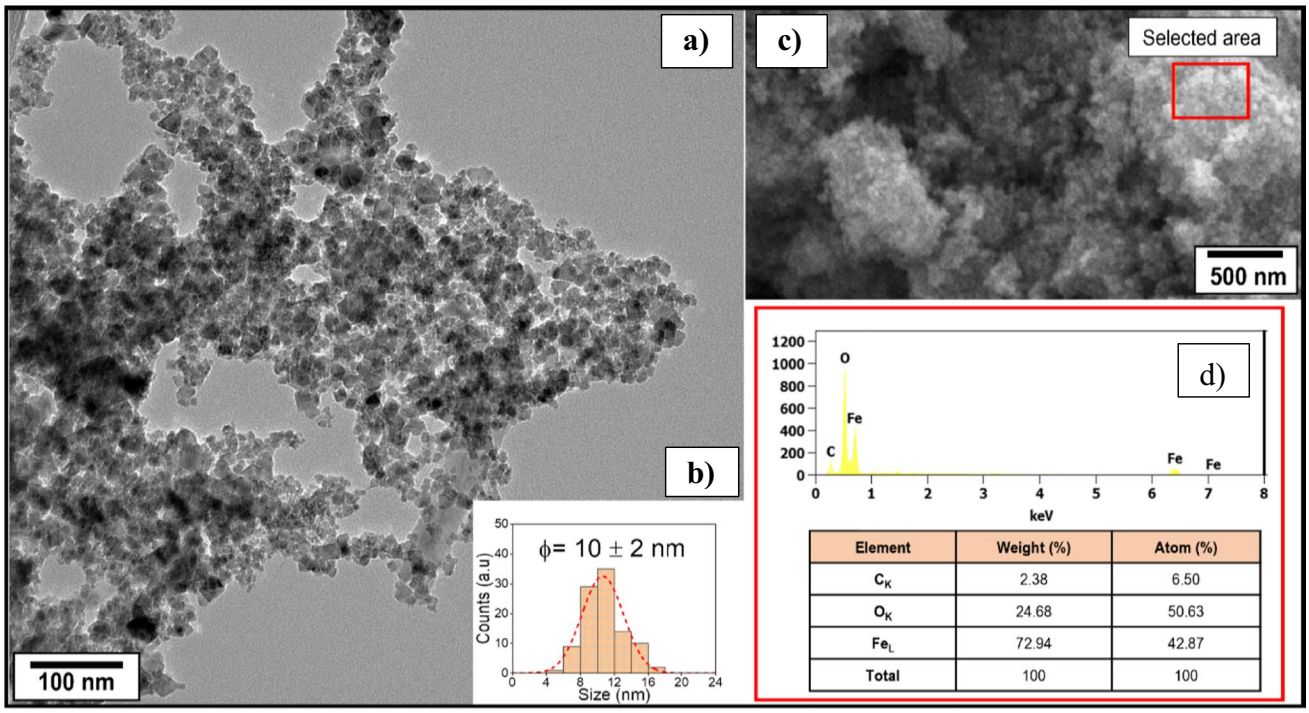

Fig. 2 Electron microscopy analysis from MNPs. Typical TEM image from MNPs (**a**), size distribution histogram (n = 200) from TEM image analysis (**b**), SEM image showing MNP agglomerates (**c**), and EDS spectrum (recorded at 10 kV) with the compositional table results (**d**)

It is reported that magnetism is size-dependent; the particle size must reach a small diameter, the so-called critical small diameter "D" [34]. It is well known that particles with an average diameter of up to 100 nm are generally referred to as bulk material; while below this size particles belong to the category of NPs. Wallyn et al. reveal that bulk materials made of ferromagnetic, ferrimagnetic, or antiferromagnetic particles have a microstructure composed of many magnetic domains, called Weiss domains, separated by walls, named Bloch walls. These domain walls are designed to reduce magnetic stray energy [34]. Thus, in each domain of the particle, a collective coupling of spins makes the spins is collinear along one direction due to the magnetic anisotropy energy [35–37]. On the contrary, for NPs, the magnetization is uniform in any of them but different from one domain to another one. Thus, at room temperature and under zero magnetic field, all domains have their own spin alignment rendering the bulk material macroscopically non-magnetic or with a global magnetization near zero due to the balance of every Weiss domains' magnetism by their next neighbor domains. However, applying an external magnetic field can induce wall movement—or in other words domain nucleation. In the case of a small magnetic field or, in the case of an intense magnetic field, this causes each spin of each single Weiss domain rotate away from their easy axis magnetization and be reoriented along an unique and same direction aiming to turn the bulk material in to a magnet. This uniform and finite magnetization persist as long as the magnetic field is applied and stops right after its removal [36–38]. These statements confirmed the study done by Morrish and Yu who determined that a single-domain magnetite particle is achieved when the diameter of particle is less than 50 nm [39]. However, in other literature, iron oxides and the magnetic particles in general become single domain when the particles size is smaller than 100 nm, and this limit is a function of material properties [40]. According to Sunaryono et al., the magnetization has particular relation between the coercivity field and the particle size, which is associated with the theory of magnetic domains. They have also revealed that the magnetic properties of samples increases with increasing particles size [41]. In the Ismail study, the effect of sintering temperature and times which affect the microstructure characteristic by increasing grain size and leads to abnormal grains and pores then the decrease in density, thus decreases the magnetic properties, mainly the volume magnetization and the magnetic induction. They attributed the nonlinear relationship to the characteristic of the transition from single-domain to multi-domain grains [42]. This phenomenon is particularly evident in the coercivity values versus particle or grain size of the magnetic material [43]. According to Lin et al., for MNPs prepared by mechanochemical reaction, the coercivity (*Hc*) initially increases with decreasing crystallite size, reaching a maximum value of 110 Oe at 22.2 nm and then decreases for each further decrease in particle size [44]. Therefore, the particle size of synthesized magnetite may be adequate for the treatment of polluted water by coupling with an intense magnetic system.

3.1.2 FTIR spectra

Figure 3 displays the FTIR spectra of the MNPS samples. It exhibits a noticeable absorption band at 538 cm^{-1}, corresponding to the stretching of Fe-O functional groups inherent to the magnetite lattice (Fe_3O_4).

Another important result is the absence of vibration mode of Fe^{II}-O assigned to maghemite, which appears generally at 613.32 cm^{-1}, 509.17 cm^{-1}, and mentioned in the literature. This result clearly shows that the obtained nano-product is composed only by pure magnetite.

O-H bending vibration and hydrogen-bonded water molecules adhering to the surface are responsible for two more vibration bands that are located at 3411 cm^{-1} and 1636 cm^{-1} [35].

The outcomes of this research are in agreement with earlier studies that identified a broad and intense absorption peak within the range of 540 to 630 cm^{-1}, which corresponds to Fe-O bonds in bulk magnetite.

Waldron's work is cited by [36] findings support the notion that magnetite can form crystals with interconnected structures, where atoms are bonded by balanced forces such as ionic, covalent, or van der Waals interactions. The observed outcomes suggest that vibrational modes of the Fe-O bond are linked to octahedral and tetrahedral sites, manifesting around 440 cm^{-1} and 560 cm^{-1}, respectively.

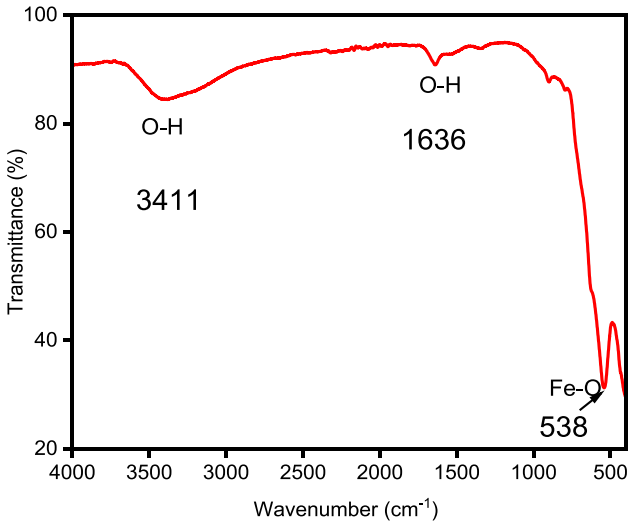

Fig. 3 FTIR spectra of MNP samples. The main interactions between hydroxyl groups (3411 and 1636 cm^{-1}) and Fe (538 cm^{-1}) were detected

3.1.3 (BET) surface area analysis

The MNPs underwent analysis using the BET technique to ascertain the specific surface area and distribution of porosity within the powder. These parameters are crucial for adsorbing pollutants in polluted water and enabling the removal of various molecules. The resulting BET surface area was 121.44 ± 0.14 m^2/g. The pore volume measures approximately 0.28cm^3/g, and the pore diameter is 10.30nm.

As depicted in Fig. 4, the acquired MNPs exhibit characteristics akin to a type III isotherm, where the adsorbate-adsorbate interaction dominates while the substrate exerts weak interactions. However, the BET surface area is considerable and suitable for adsorption in heterogeneous surfaces.

3.1.4 Thermal analysis

Figure 5 depicts the thermogravimetric analysis (TGA) curve of the Fe_3O_4 precursor. The TGA curve in the thermogram shows two distinct mass loss phases. Between 50 and 300 °C, the initial mass loss phase is slow. The removal of surface adsorbed water was responsible for the mass loss, which was 3.80%.

The removal of physically adsorbed water during the decomposition of Fe_3O_4 is revealed by the second stage of mass loss, which occurs between 300 and 500°C and indicates a mass loss of 1.80%. The weight of the magnetite nanoparticles was nearly constant above 500°C, but an exothermic peak was observed around 600°C, indicating a phase transition from Fe_3O_4 to Fe_2O_3. The phase transition was carried out at temperatures between 550 and 700°C.

3.1.5 XRD analysis

Figure 6 illustrates the XRD patterns of the magnetite nanoparticles. All diffraction peaks are cataloged according to the magnetite (Fe_3O_4) ICSD pattern with the number 01-080-0390. The findings in the ICSD pattern of magnetite (Fe_3O_4) [37–50] are consistent with this outcome.

The produced magnetite has a cubic spinel structure, according to the Fe_3O_4 NP XRD pattern recorded in the literature [51]. The crystalline and high purity of magnetite with nanoparticles size were confirmed by the extent of peak broadening and the absence of unaccounted peaks. Using Debye equation Scherrer's (1), the average crystal size of the magnetite nanoparticles was approximated [52].

$$D = \frac{K * \lambda}{\beta * \cos\theta} \tag{1}$$

where D represents the average crystal size, λ signifies the wavelength of the X-ray radiation (1.5406 Å), K denotes the dimensionless form factor (0.9), θ signifies the Bragg's angle

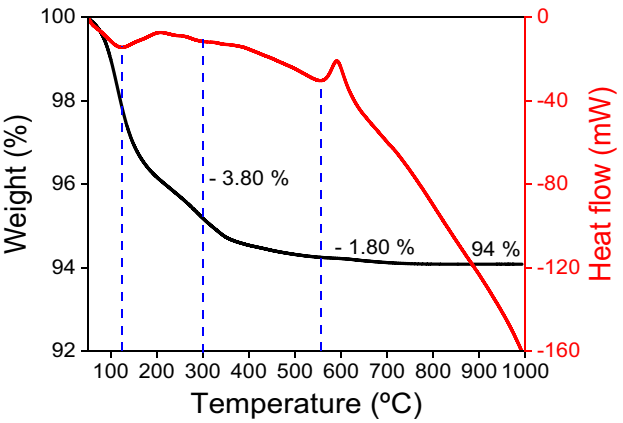

Fig. 5 Thermogravimetric analysis of FeO_4 nanostructures

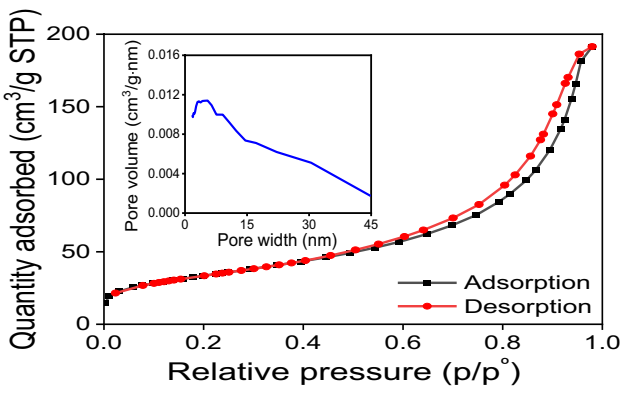

Fig. 4 Performing BET analysis and constructing nitrogen adsorption–desorption isotherms, followed by the creation of pore size distribution curves

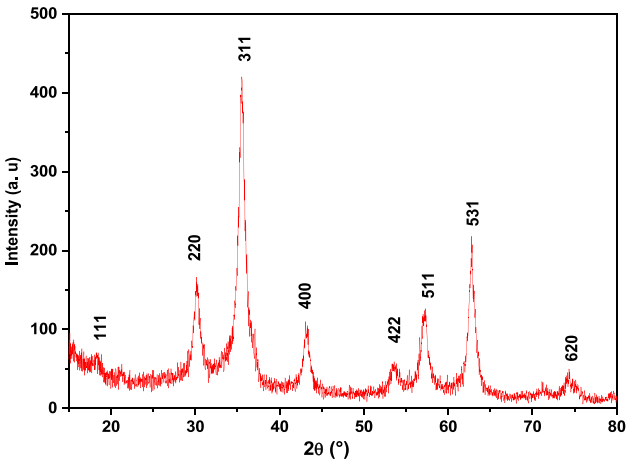

Fig. 6 Structural analysis of FeO_4 nanoparticles via X-ray diffraction

in degrees, and β signifies the line's FWHM (full width at half maximum) in radians [53].

The FWHM of the Fe_3O_4 prominent peak (2 = 35.466°) of XRD patterns, which corresponds to the plane, was used to estimate the mean crystalline size (100). The average crystal size of the synthesized nanomaterials is ~10 nm.

3.2 MNPs as water quality enhancement agents

3.2.1 Impacts of contact duration

The influence of contact time on the efficiency of BOD_5 and COD removal was initially tested for 177 and 56.5 mg/L, respectively, at times (15, 30, 45, 60, and 90 min) with 1 g of magnetite NPs due to the significance of contact time on the reduction of COD and BOD_5 by magnetite. The pH of the contaminated water was kept at 8, stirring occurred at approximately 200 rpm, and the ambient temperature was maintained at 20±1°C. The results obtained showed a high level of COD and BOD_5 removal reaching 61% within 50 min. This implies that in order to achieve optimal efficiency, the contact time should be set to a minimum of 50 min (Fig. 7). Nevertheless, the outcomes revealed that the removal efficiency for COD and BOD_5 reached a plateau following a contact time of 50 min. After 60 min, the equilibrium time of treatment is attained because the absorption capacity of COD and BOD_5 has remained constant. According to the study carried out by [54], the impact of MNPs treatment on polluted water was demonstrated by synthesizing nanoparticles using the combustion method, with a diameter of 17 nm. It was concluded that the optimum time for achieving maximum efficiency in reducing COD and BOD_5 was 80 min. These results suggest that the diameter of the nanoparticles and the method of synthesis influence the time required to achieve maximum efficiency in reducing pollution, underlining the importance of these parameters in the treatment process.

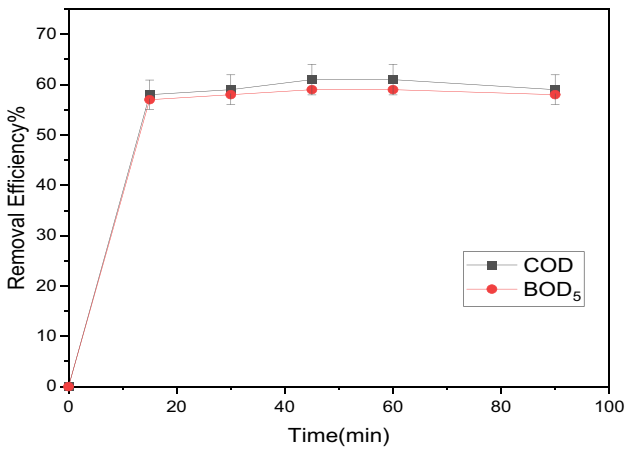

Fig. 7 Impact of contact time on removal efficiency

3.2.2 Effect of iron oxide nanoparticles concentration

Figure 8 shows the removal efficiency of COD and BOD_5 from water contaminated with different concentrations of iron oxide nanoparticles. The results indicate that the adsorption efficiency of COD increased from 40 to 65% when the dosage of Fe_3O_4-MNP was increased from 0.5 to 1.5 g/L, and that the value remained unchanged from the mass of 0.8 g/L. For BOD_5, the removal efficiency increased from 64 to 65% in the range from 0.8 to 1 g/L and decreased with increasing magnetite dosage. This can be due to the fact that a rise in adsorbent dose causes a rise in the amount of nanoparticle active sites and the specific adsorption surface, which causes a significant increase in the nanoparticle molecules' capacity for adsorption on magnetite surfaces.

3.2.3 Effect of pH

Experiments were performed in neutral acidic and alkaline media with BOD_5 and COD concentrations (177 and 56.5 mg/L), pH values (4, 6, 7, 8, and 9) using 0.8 g/L. Fe_3O_4 NPs, contact time 50 min, stirring rate 200 rpm, and ambient temperature 25 ± 1 °C.

At equilibrium, the removal efficiencies of COD and BOD_5 were (61, 62.2, 63.4, 64.4, and 63.8%), respectively and (60.8, 63, 64.2, 65, and 64.8%), in this order as shown Fig. 9.

The outcomes revealed that the peak removal efficiency occurred at a pH of 8, within weakly alkaline conditions.

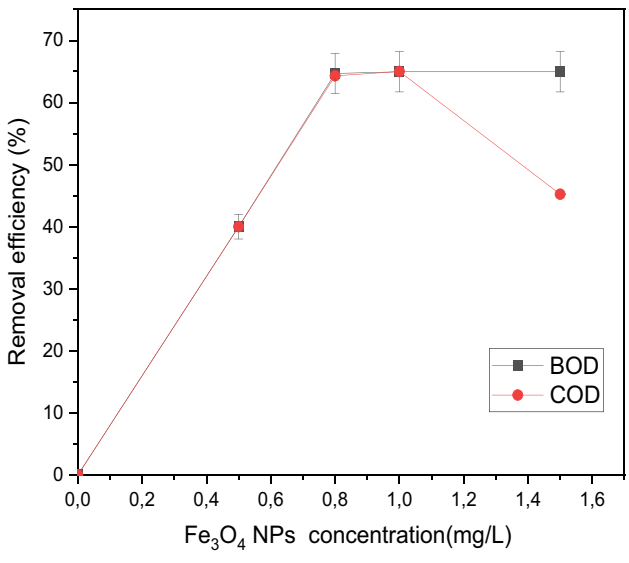

Fig. 8 Effect of iron oxide nanoparticle concentrations on the removal efficiency

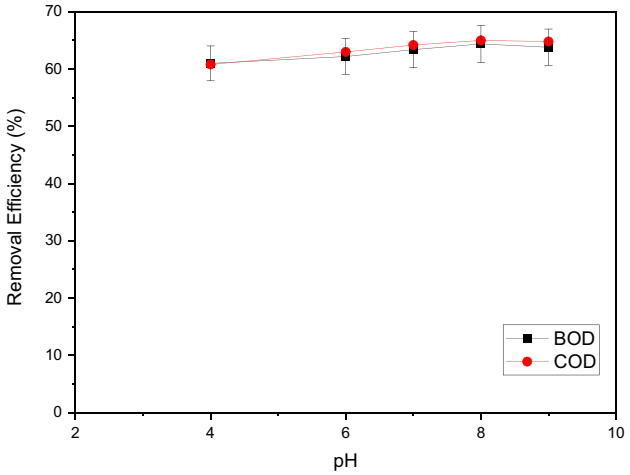

Fig. 9 Effect of pH value on removal efficiency

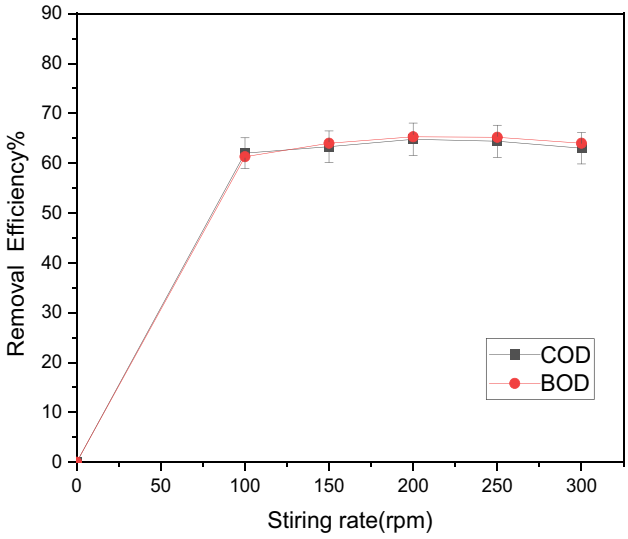

Fig. 10 Influence of stirring rate on the removal efficiency

This finding is attributable to the behavior of small magnetite particles in highly acidic environments; they degrade due to the influence of acid, resulting in nanoparticles with vacant sites that affect adsorption activity. Conversely, in strongly alkaline solutions, an abundance of OH^- ions can intensify the removal rate of COD and BOD_5 by activating adsorption sites for negatively charged ions. Notably, numerous researchers have observed similar outcomes using varied adsorbent materials for polluted water treatment, thus highlighting the efficacy of pH = 8.

3.2.4 Impact of stirring rate

Stirring speed affects the adsorption efficiency and is a crucial parameter in the investigation of COD and BOD_5 removal. In this study, the concentration of magnetite was 0.8 g/L, pH 8, room temperature (25 ± 1 °C) and stirred for 50 min to study the effect of stirring speed on the efficiency of removal of COD and BOD_5 under the concentration of 177 and 56.5 mg/lift. According to Fig. 10, the elimination efficiencies for BOD_5 and COD were, respectively, 62, 63.3, 64.8, 64.4, and 63% and 61.3, 64, 65.3, 65.2, and 64%, respectively. According to the results, 200 rpm was the ideal stirring speed, while stirring speeds above this point may not result in increased removal efficiency.

Based on the research conducted by [54], it was found that a stirring rate of 250 rpm is ideal for achieving the highest efficiency in reducing COD and BOD_5 levels. These findings indicate that the size of nanoparticles and the synthesis method have an impact on the time needed to reach peak pollution reduction efficiency, highlighting the significance of these factors in the treatment procedure.

3.3 Coupling adsorption and magnetic separation for the reduction of COD and BOD_5

After identifying the optimal conditions for water treatment, the ideal parameters were defined as follows: a contact time of 50 min, a concentration of 0.8 g/L of iron oxide nanoparticles, a pH of 8, and a mixing speed of 200 rpm. Under these conditions, the treatment of polluted water using iron oxide nanoparticles (MNPs), without magnetic coupling, resulted in a significant COD reduction (64%) and a BOD_5 reduction (65%). Subsequently, additional treatment was conducted by introducing a magnetic field using an intensity of 1 Tesla combined with the nanoparticle treatments under the determined optimal conditions. The results showed a significant improvement, with a decrease of 84% in COD and 85% in BOD_5, indicating a reduction improvement of 20%. These findings are consistent with our previous study [54], which examined the impact of MNP treatment on polluted water using magnetic coupling with a field intensity of 0.33 Tesla. The results of this study revealed a reduction of 76% in COD and 78% in BOD_5, confirming that the higher the magnetic intensity is, the more significant the reduction in contaminants becomes. Based on these studies, the application of a high-intensity magnetic field can improve the removal of COD and BOD_5 from polluted water. When magnetic fields are combined with Fe_3O_4 nanoparticles, removal efficiency can significantly improve.

Furthermore, the specific outcomes of this investigation highlight the efficiency of magnetic nanoparticles synthesized via the co-precipitation method. The highest reduction efficiencies of 84% for COD and 85% for BOD_5 were achieved after 50 min of contact time, at a pH of 8, using 1g/l of MNPs,

and a stirring rate set at 200 rpm. In addition, the application of a magnetic field with an intensity of 1 T significantly enhanced the removal efficiencies.

4 Conclusions

The co-precipitation method for synthesizing magnetite nanoparticles appears promising as an adsorbent for removing organic compounds from contaminated water. During the experiments, a significant reduction of 64% for COD and 65% for BOD5 was achieved in just 50 min, using optimal conditions such as a pH of 8, a concentration of magnetite nanoparticles at 0.8 g/l, and an agitation speed of 200 revolutions per minute.

However, the most significant advancement came from using a very strong magnetic field of 1 Tesla (DELTA WATER) under the same optimal conditions. This innovative approach significantly boosted the reduction efficiency, increasing it from 20% to a remarkable 84% for COD and reaching an impressive 85% for BOD5. The use of this high-intensity magnetic field opens up new possibilities in the treatment of contaminated water, highlighting its substantial potential for more effective removal of organic contaminants.

Acknowledgements We would like to express our sincere gratitude to Prof. Jesús Antonio Fuentes-García and Prof. Gerardo F. Goya from the Instituto de Nanociencia y Materiales de Aragón (INMA), CSIC-Universidad de Zaragoza, Campus Río Ebro, 50018, Zaragoza, Spain, for their invaluable contributions to the data collection process and their assistance in data analysis and interpretation, which greatly enhanced the depth and quality of our research results. We wish also to thank Ministry of Higher Education and Scientific Research Tunisia for their continuous encouragement by project of young researcher 20PJEC04-03. On the other hand, we thank the company "Delta Water" for the devices dedicated to testing, and our sincere thanks to Prof. Ahmed Ibrahim and Prof. Sherif Ibrahim for granting the devices to perform the experimental test.

Author contributions Conceptualization: HT, AE, MF; methodology: HT, NA, AE, MF; validation: NA, AE, MF; investigation: HT, NA; writing—original draft preparation: HT; review and editing: AE, MF, KHN; supervision: MF; all authors have read and agreed to the published version of the manuscript.

Funding Not applicable.

Data availability Data sharing is not applicable to this article as no datasets were generated or analyzed during the current study.

Declarations

Competing interests The authors declare no competing interests.

References

1. L. Fan, J. Xie, Z. Zhang, Y. Zheng, D. Yao, T. Li, Magnetically recoverable Fe3O4@polydopamine nanocomposite as an excellent co-catalyst for Fe3+ reduction in advanced oxidation processes. J. Environ. Sci (China). **92**, 69–78 (2020). https://doi.org/10.1016/j.jes.2020.02.006
2. Y.H. Huang, T.C. Zhang, P.J. Shea, S.D. Comfort, Effects of oxide coating and selected cations on nitrate reduction by iron metal. J. Environ. Qual. **32**, 1306 (2003). https://doi.org/10.2134/jeq2003.1306
3. L. Ma, L. Zhang, Enhanced biological treatment of industrial wastewater with bimetallic zero-valent iron. Environ. Sci. Technol. **42**(5384–5389) (2008). https://doi.org/10.1021/es801743s
4. I. De Vicente, A. Merino-Martos, F. Guerrero, V. Amores, J. de Vicente, Chemical interferences when using high gradient magnetic separation for phosphate removal: consequences for lake restoration. J. Hazard. Mater. **192**, 995–1001 (2011). https://doi.org/10.1016/j.jhazmat.2011.05.090
5. M. Gavrilescu, Water, soil, and plants interactions in threatened environment. Water. **13**, 2746 (2021). https://doi.org/10.3390/w13192746
6. X. Bao, Z. Qiang, J.H. Chang, W. Ben, J. Qu, Synthesis of carbon-coated magnetic nanocomposite (Fe3O4 at C) and its application for sulfonamide antibiotics removal from water. J. Environ. Sci (China). **26**, 962–969 (2014). https://doi.org/10.1016/S1001-0742(13)60485-4
7. I. Ali, T.A. Khan, M. Asim, Removal of arsenic from water by electrocoagulation and electrodialysis techniques. Sep. Purif. Rev. **40**, 25–42 (2011). https://doi.org/10.1080/15422119.2011.542738
8. V.K. Gupta, A. Nayak, Cadmium removal and recovery from aqueous solutions by novel adsorbents prepared from orange peel and Fe 2O 3 nanoparticles. Chem. Eng. J. **180**, 81–90 (2012). https://doi.org/10.1016/j.cej.2011.11.006
9. T.A. Saleh, V.K. Gupta, Functionalization of tungsten oxide into MWCNT and its application for sunlight-induced degradation of rhodamine B. J. Colloid. Interface Sci. **362**, 337–344 (2011). https://doi.org/10.1016/j.jcis.2011.06.081
10. S. Nagib, R.S.A. Hameed, Recovery of vanadium from hydrodesulfurization waste catalyst using calix resorcinarenes. Green Chem. Lett. Rev. **10**(4), 210–215 (2017). https://doi.org/10.1080/17518253.2017.1348543
11. M. Bhavisha, S. Balamurugan, S.A. Ashika, N.J. Venkatesha, T. Maiyalagan, Combustion synthesis of copper-doped perovskite $SrFe_{1-X}Cu_xO_{3-\delta}$ nanomaterials and its potential application on hydroxylation. Mater Today Sustain of Anisole, a Biomass Model Component. Mater. Today Sustain. **21**, 100266 (2023). https://doi.org/10.1016/j.mtsust.2022.100266
12. R. Ranga, A. Kumar, P. Kumari, P. Singh, V. Madaan, Ferrite application as an electrochemical sensor: a review. Mater. Charact. **178**, 111269 (2021). https://doi.org/10.1016/j.matchar.2021.111269
13. M. Bhavisha, S. Aswani, D.A. Sreenavya, P.P. Neethu, I.G. Archana, Molybdenum incorporated strontium-iron and strontium-cobalt ($SrBMoO_{3-\delta}$; B=Fe & Co) perovskites: preparation and their application on oxidation of iso-eugenol into vanillin. Eur. J. Inorg. Chem. **26** (2023). https://doi.org/10.1002/ejic.202200590
14. T. Tanaka, T. Matsunaga, Fully automated chemiluminescence immunoassay of insulin using antibody - protein A - bacterial magnetic particle complexes. Anal. Chem. **72**, 3518–3522 (2000). https://doi.org/10.1021/ac9912505
15. P. Marcinowski, D. Bury, M. Krupa, D. Ścieżyńska, P. Prabhu, J. Bogacki, Magnetite and hematite in advanced oxidation processes application for cosmetic wastewater treatment. Processes. **8**, 1–17 (2020). https://doi.org/10.3390/pr8111343
16. A. Gallo-Cordova, M.D.M. Silva-Gordillo, G.A. Muñoz, X. Arboleda-Faini, D. Almeida Streitwieser, Comparison of the adsorption capacity of organic compounds present in produced water with commercially obtained walnut shell and residual biomass. J. Environ. Chem. Eng. **5**, 4041–4050 (2017). https://doi.org/10.1016/j.jece.2017.07.052

17. S. Uk, T. Ne, Efficient magnetic capture of PE microplastic from water by PEG modified Fe_3O_4 nanoparticles : performance, kinetics, isotherms and influence. J. Environ. Sci. (2023). https://doi.org/10.1016/j.jes.2023.07.025
18. Z. Hajahmadi, H. Younesi, N. Bahramifar, H. Khakpour, K. Pirzadeh, Multicomponent isotherm for biosorption of Zn(II), CO(II) and Cd(II) from ternary mixture onto pretreated dried *Aspergillus niger* biomass. Water Resour. Ind. **11**, 71–80 (2015). https://doi.org/10.1016/j.wri.2015.07.003
19. K. Pirzadeh, A.A. Ghoreyshi, Phenol removal from aqueous phase by adsorption on activated carbon prepared from paper mill sludge. Desalin Water Treat. **52**, 6505–6518 (2014). https://doi.org/10.1080/19443994.2013.821034
20. A.R. Mahdavi, A.A. Ghoresyhi, A. Rahimpour, H. Younesi, K. Pirzadeh, COD removal from landfill leachate using a high-performance and low-cost activated carbon synthesized from walnut shell. Chem. Eng. Commun. **205**, 1193–1206 (2018). https://doi.org/10.1080/00986445.2018.1441831
21. A.M. Muliwa, T.Y. Leswifi, M.S. Onyango, A. Maity, Magnetic adsorption separation (MAS) process: an alternative method of extracting Cr(VI) from aqueous solution using polypyrrole coated Fe3O4 nanocomposites. Sep. Purif. Technol. **158**, 250–258 (2016). https://doi.org/10.1016/j.seppur.2015.12.021
22. R.M. Dias, J.G. Silva, V.L. Cardoso, M.M. de Resende, Removal and desorption of chromium in synthetic effluent by a mixed culture in a bioreactor with a magnetic field. J. Environ. Sci. (China) **91**, 151–159 (2020). https://doi.org/10.1016/j.jes.2020.01.026
23. H. Ben Amor, A. Elaoud, K. Elmoueddeb, Influence of magnetic field on water characteristics and potato cultivation influence of magnetic field on water characteristics and potato cultivation. J. Agric. Environ. Sci. **16**, 32–41 (2018)
24. A. Elaoud, N. Turki, H. Ben Amor, R. Jalel, N. Ben Salah, Influence of the magnetic device on water quality and production of melon. (2016). https://doi.org/10.14741/Ijcet/22774106/6.6.2016.48
25. H. Ben Amor, A. Elaoud, M. Hozayn, Does magnetic field change water pH ?. Asian Research. J. Agric. **8**, 1–7 (2018). https://doi.org/10.9734/ARJA/2018/39196
26. H. Ben Amor, A. Elaoud, H. Ben Hassen, N. Ben Salah, A. Masmoudi, K. Elmoueddeb, Characteristic study of some parameters of soil irrigated by magnetized waters. Arab J. Geosci. **13** (2020). https://doi.org/10.1007/s12517-020-06015-0
27. H. Ben Hassen, M. Hozayn, A. Elaoud, A. Attia Abdd El-monem, Inference of magnetized water impact on salt-stressed wheat. Arab J. Sci. Eng. **45**, 4517–4529 (2020). https://doi.org/10.1007/s13369-020-04506-6
28. H. Ben Amor, A. Elaoud, N. Ben Salah, K. Elmoueddeb, Effect of magnetic treatment on surface tension and water evaporation. Int. J. Adv. Ind. Eng. 3–9 (2017). https://doi.org/10.14741/Ijae/5.3.4
29. A.M. Atta, R.S. Abdel Hameed, H.A. Al-Lohedan, A.O. Ezzat, A.I. Hashem, Magnetite doped cuprous oxide nanoparticles as modifier for epoxy organic coating. Prog. Org. Coat. **112**(295–303) (2017). https://doi.org/10.1016/j.porgcoat.2017.07.018
30. M. Khatamian, B. Divband, R. Shahi, Ultrasound assisted co-precipitation synthesis of Fe3O4/ bentonite nanocomposite: performance for nitrate, BOD and COD water treatment. J. Water Process. Eng. **31**, 100870 (2019). https://doi.org/10.1016/j.jwpe.2019.100870
31. R.H. Hesas, M.S. Baei, H. Rostami, J. Gardy, A. Hassanpour, An investigation on the capability of magnetically separable Fe3O4/ mordenite zeolite for refinery oily wastewater purification. J. Environ. Manag. **241**, 525–534 (2019). https://doi.org/10.1016/j.jenvman.2018.09.005
32. S.S. Shafqat, A.A. Khan, M.N. Zafar, M.H. Alhaji, K. Sanaullah, S.R. Shafqat, S. Murtaza, S.C. Pang, Development of amino-functionalized silica nanoparticles for efficient and rapid removal of COD from pre-treated palm oil effluent. J. Mater. Res. Technol. **8**(385–395) (2019). https://doi.org/10.1016/j.jmrt.2018.03.002
33. D.H. Chen, S.H. Wu, Synthesis of nickel nanoparticles in water-in-oil microemulsions. Chem. Mater. **12**, 1354–1360 (2000). https://doi.org/10.1021/cm991167y
34. J. Wallyn, N. Anton, T.F. Vandamme, Synthesis, principles, and properties of magnetite nanoparticles for in vivo imaging applications—a review. Pharmaceutics. **11**(601) (2019). https://doi.org/10.3390/pharmaceutics11110601
35. A.H. Lu, E.L. Salabas, F. Schüth, Magnetic nanoparticles: synthesis, protection, functionalization, and application. Angew. Chem. Int. Ed. **46**, 1222–1244 (2007)
36. G.C. Papaefthymiou, Nanoparticle magnetism. Nano Today. **4**, 438–447 (2009)
37. S. Kamali, T. Ericsson, R. Wäppling, Characterization of iron oxide nanoparticles by Mössbauer spectroscopy. Thin. Solid. Films. **515**, 721–723 (2006)
38. N.A. Frey, S. Peng, K. Cheng, S. Sun, Magnetic nanoparticles: synthesis, functionalization, and applications in bioimaging and magnetic energy storage. Chem. Soc. Rev. **38**, 2532–2542 (2009)
39. A.H. Morrish, S.P. Yu, Magnetic measurements on individual microscopic ferrite particles near the single-domain size. Phys. Rev. **102**, 670–673 (1956)
40. R.M. Cornell, U. Schwertmann, *Electronic, electrical and magnetic properties and colour, in The Iron Oxides* (Wiley-VCH Verlag GmbH & Co. KGaA, 2004), pp. 111–137
41. Sunaryono, A. Taufiq, Mashuri, S. Pratapa, M. Zainuri, Triwikantoro, Darminto, Various magnetic properties of magnetite nanoparticles synthesized from iron-sands by coprecipitation method at room temperature. Mater. Sci. Forom **827**, 229–234 (2015). https://doi.org/10.4028/www.scientific.net/MSF.827.229
42. I. Ismail, I. Riati Ibrahim, R. Nazlan, *Evolution of magnetic properties in ferrites: trends of single-sample and multi-sample sintering* (INTECH, 2018). https://doi.org/10.5772/intechopen.68500
43. M. Rahimi, P. Kameli, M. Ranjbar, H. Salamati, The effect of sintering temperature on evolution of structural and magnetic properties of nanostructured $Ni_{0.3}Zn_{0.7}Fe_2O_4$ ferrite. J. Nanopart. Res. **15**, 1865–1876 (2013). https://doi.org/10.1007/s11051-013-1865-1
44. C.-R. Lin, Y.-M. Chu, S.-C. Wang, Magnetic properties of magnetite nanoparticles prepared by mechanochemical reaction. Mater. Lett. **60**, 447–450 (2006)
45. T. Seki, K.Y. Chiang, C.C. Yu, X. Yu, M. Okuno, J. Hunger, Y. Nagata, M. Bonn, The bending mode of water: a powerful probe for hydrogen bond structure of aqueous systems. J. Phys. Chem. Lett. **11**, 8459–8469 (2020). https://doi.org/10.1021/acs.jpclett.0c01259
46. S. Aliramaji, A. Zamanian, Z. Sohrabijam, Characterization and synthesis of magnetite nanoparticles by innovative sonochemical method. Procedia. Mater. Sci. **11**(265–269) (2015). https://doi.org/10.1016/j.mspro.2015.11.022
47. A.J.S. Ahammad, J. Lee, A. Rahman, Electrochemical sensors based on carbon nanotubes 2289–2319 (2009). https://doi.org/10.3390/s90402289
48. F.G. Sánchez, A.N. Dıaz, M.R. Peinado, C. Belledone, Free and sol–gel immobilized alkaline phosphatase-based biosensor for the determination of pesticides and inorganic compounds. Anal. Chim. Acta. **484**(1), 45–51 (2003). https://doi.org/10.1016/S0003-2670(03)00310-6
49. B.W. Lu, W.C. Chen, A disposable glucose biosensor based on drop-coating of screen-printed carbon electrodes with magnetic nanoparticles. J. Magn. Magn. Mater. **304**, 400–402 (2006). https://doi.org/10.1016/j.jmmm.2006.01.222

50. S. Sun, H. Zeng, D.B. Robinson, S. Raoux, P.M. Rice, S.X. Wang, G. Li, Monodisperse MFe_2O_4 (M) Fe , Co , Mn. Nanoparticles. **4**, 126–132 (2004)
51. T.Y. Kim, M.S. Lee, Y. Il Kim, C.S. Lee, J.C. Park, D. Kim, The enhanced anisotropic properties of the Fe3-xMxO4 (M = Fe, Co, Mn) films deposited on glass surface from aqueous solutions at low temperature. J. Phys. D. Appl. Phys. **36**, 1451–1457 (2003). https://doi.org/10.1088/0022-3727/36/13/303
52. M. Qayoom, R. Bhat, K. Asokan, M.A. Shah, G.N. Dar, Unary doping effect of A 2 + (A = Zn , Co , Ni) on the structural , electrical and magnetic properties of substituted iron oxide nanostructures. J. Mater. Sci. Mater. Electron. **31**, 8268–8282 (2020). https://doi.org/10.1007/s10854-020-03362-2
53. A. Ali, Y.W. Chiang, R.M. Santos, X-ray diffraction techniques for mineral characterization: a review for engineers of the fundamentals, applications, and research directions. Minerals. **12**, 205 (2022). https://doi.org/10.3390/min12020205
54. H. Tlili, A. Elaoud, N. Asses, K. Horchani-naifer, M. Ferhi, Reduction of oxidizable pollutants in waste water from the Wadi El Bey River basin using magnetic nanoparticles as removal agents. Magnetochemistry. **9**, 157 (2023)